A Multimodal Robot for Perching and Climbing on Vertical Outdoor Surfaces

Morgan T. Pope, Christopher W. Kimes, Hao Jiang, Elliot W. Hawkes, *Student Member, IEEE*, Matt A. Estrada, Capella F. Kerst, William R. T. Roderick, Amy K. Han, David L. Christensen, and Mark R. Cutkosky, *Fellow, IEEE*

***Abstract*—Perching can extend the useful mission life of a micro air vehicle. Once perched, climbing allows it to reposition precisely, with low power draw and without regard for weather conditions. We present the Stanford Climbing and Aerial Maneuvering Platform, which is to our knowledge the first robot capable of flying, perching with passive technology on outdoor surfaces, climbing, and taking off again. We present the mechanical design and the new perching, climbing, and takeoff strategies that allow us to perform these tasks on surfaces such as concrete and stucco, without the aid of a motion capture system or off-board computation. We further discuss two new capabilities uniquely available to a hybrid aerial–scansorial robot: the ability to recover gracefully from climbing failures and the ability to increase usable foothold density through the application of aerodynamic forces. We also measure real power consumption for climbing, flying, and monitoring and discuss how future platforms could be improved for longer mission life.**

***Index Terms*—Climbing, failure recovery, mechanisms, micro air vehicles (MAVs), microspines, perching, takeoff, unstructured environments.**

I. Introduction

PERCHING can allow a micro air vehicle to perform useful sensing tasks over long periods of time by eliminating the high power draw necessary for continuous flying. Adding the ability to climb allows a perched robot to survey a surface and reposition itself accurately regardless of weather conditions. In recent years, researchers have implemented a variety of perching strategies [1]–[9]. Previous work has also developed a flightless robot capable of perching and climbing on smooth clean surfaces [10]; other teams have developed strategies for using rotors to press wheels against a vertical surface and then use continued thrust to maintain contact with the wall and roll along the surface [11], [12]. In [13], a platform was developed that could climb on a prepared surface and then detach from the surface and enter a gliding trajectory. To our knowledge, no previous robot has been developed that is capable of flying, perching with passive attachment technology, climbing, and taking off again in outdoor operations. This paper presents such a robot, i.e., the Stanford Climbing and Aerial Maneuvering Platform (SCAMP, shown in Fig. 1), which can perch and climb on unprepared surfaces such as concrete and stucco walls.

We first describe the mechanisms and strategies that enable SCAMP's ability to perch, climb, and take off using only on-board sensing and computation. We then discuss two examples of rotor-assisted climbing, which demonstrate how rotors can enhance the operation of a climbing robot: by changing the effective loading angle to increase usable foothold density, and by allowing the robot to reattach after a failed step. Finally, we evaluate how perching and climbing can extend the mission life of our flying platform by measuring real power draw and discuss future improvements to increase efficiency.

II. Mechanism Design and Strategies for Perching, Climbing, and Takeoff

A. Mechanism Design

SCAMP is constructed by adding a two-degree-of-freedom climbing mechanism to the commercially available Crazyflie quadrotor [14]. The mechanism (see Fig. 2) is designed to rotate SCAMP into the correct orientation for perching when it impacts the wall, to move SCAMP's two spiny feet through a desired climbing gait while keeping forces within the limits of the microspines, and to enable detachment and resumption of flight when desired.

The mechanism is built around a carbon fiber frame that acts as SCAMP's spine and tail, built out of unidirectional pultruded carbon fiber rods lashed together with Kevlar thread and secured with cyanoacrylate adhesive. To perch, SCAMP flies "tail first" into a wall. As the tail makes contact, the rotors continue to turn, causing it to pitch up, into the vertical configuration shown in Fig. 2. As with other climbing robots [10], [15], the tail reduces the inward normal force required at the front feet to counteract the pitch-back moment produced by having a center of mass some distance out from the wall. The tail is equipped

Manuscript received March 3, 2016; revised June 30, 2016; accepted August 19, 2016. Date of publication December 26, 2016; date of current version February 3, 2017. This paper was recommended for publication by Associate Editor R. Carloni and Editor P. Dupont upon evaluation of the reviewers' comments. This work was supported by NSF IIS-1161679 and ARL MAST MCE 15-4.

The authors are with the Biomimetics and Dexterous Manipulation Laboratory, Center for Design Research, Department of Mechanical Engineering, Stanford University, Stanford, CA 94305-2232 USA (e-mail: mpope@stanford.edu; ckimes17@stanford.edu; jianghao@stanford.edu; ewhawkes@stanford.edu; estrada1@stanford.edu; ckerst@stanford.edu; wrtr@stanford.edu; kwhan@stanford.edu; dlcboy@gmail.com; cutkosky@stanford.edu).

This paper has supplementary downloadable material available at http://ieeexplore.ieee.org, provided by the author. The material consists of a video, viewable with QuickTime (version 7 or later) or VLC media players, providing an overview of the operation of the Stanford Climbing and Aerial Maneuvering Platform, or SCAMP. It illustrates the basic approaches to perching, climbing, failure recovery, and takeoff. The zip file (SCAMP-assembly.zip) includes the parts and assembly files for a Solidworks CAD rendering of the robot described in this paper. Contact mpope@stanford.edu for further questions about this work.

Color versions of one or more of the figures in this paper are available online at http://ieeexplore.ieee.org.

Digital Object Identifier 10.1109/TRO.2016.2623346

1552-3098 © 2016 IEEE. Personal use is permitted, but republication/redistribution requires IEEE permission.
See http://www.ieee.org/publications_standards/publications/rights/index.html for more information.

Authorized licensed use limited to: UNIVERSITA TRENTO. Downloaded on October 26,2022 at 09:44:36 UTC from IEEE Xplore. Restrictions apply.

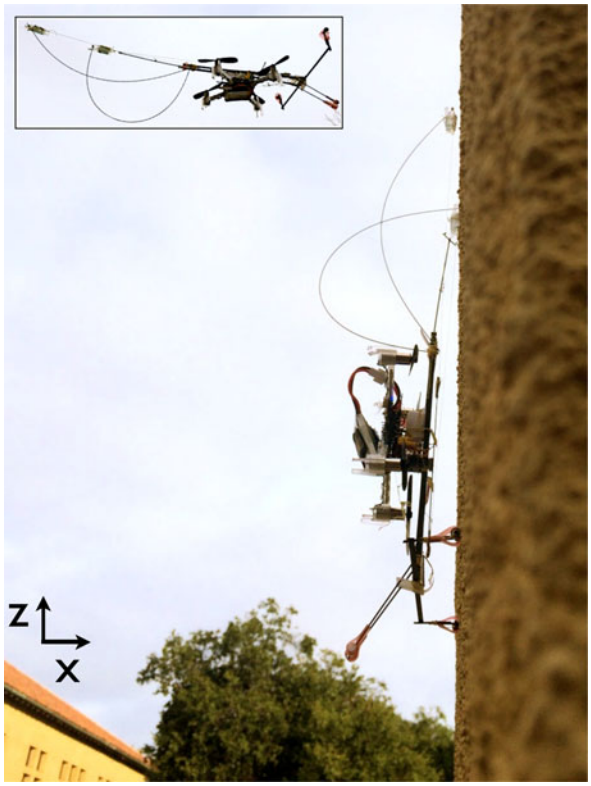

Fig. 1. SCAMP climbing the Stanford clock tower. (Inset) SCAMP in flight.

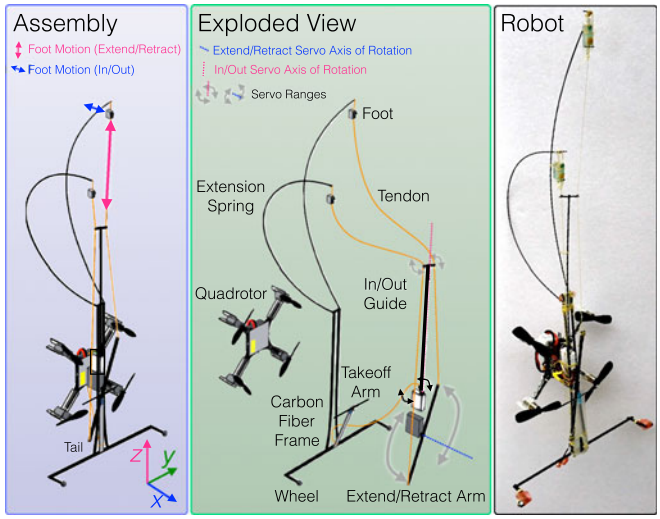

Fig. 2. (Left) CAD rendering of the SCAMP robot, with the motion range of one of the feet shown. (Middle) Exploded view of the robot, with the motion range of the two driving servos shown. The mechanism converts the rotational output of these servos into the respective linear motions of the feet. (Right) Photo of SCAMP suspended against a white background.

with miniature ball bearing "wheels" to reduce drag as it climbs and prevent catching on asperities.

Two RC servos are mounted to the frame, near the center of mass. The first servo (4 g Hitec HS-5035HD) controls the motion of the feet in the vertical direction, parallel to the climbing surface, and is called the extend/retract servo. The servo rotates a stiff carbon-fiber rod, the extend-retract arm (see Fig. 2, middle), back and forth about the x-axis, extending and retracting the feet. The second servo (2 g Hobbyking HK-5320) controls the motion of the feet in the direction normal to the climbing surface and is called the in/out servo. The in/out servo is coupled to a long T-shaped device made of carbon fiber rods, the in/out guide. The in/out guide rotates about the z-axis. The top bar of the in/out guide is equipped with small wire loops that guide tendons attached to the feet. Thus, as it rotates, a tendon is guided either along the surface (loading the spines) or slightly away from the surface (extending for the next step).

Each foot is suspended on its own tendon, which is kept in tension by a bent carbon fiber strip acting as an extension spring, with relatively constant force due to the bow-spring design [16]. The carbon fiber bow spring is attached to the frame by a pin joint, allowing it to rotate toward and away from the wall. The tendons attached to the feet are routed through the two wire loops on the in/out guide and then anchored to opposite ends of the extend/retract servo arm. When the extend/retract arm rotates, one tendon retracts the foot attached to it, while the other tendon extends, allowing the foot to move upward. Together, the in/out guide and the extend/retract servo can move the feet along nearly any 2-D path within their range of motion, allowing for an adjustable climbing gait.

Attached to the tail is a stiff spring-loaded fiberglass "takeoff arm." At the end of this arm is a single spine. When both servos are simultaneously moved to a special configuration, not encountered in normal climbing operation, the takeoff arm deploys to engage with the surface, as discussed further in Section II-D. After deployment, the takeoff arm is retracted to its normal position, tucked against the frame, using another tendon attached to the in/out servo.

The feet, frame, and extension springs weigh a total of 5 g, bringing the total mechanism weight to 11 g. The mechanism is then attached to the 27 g Crazyflie quadrotor for a total robot weight of 38 g.

B. Perching Strategy

To perch, SCAMP is directed toward a surface by a human operator. Once its tail impacts the wall, an automated routine detects the contact and turns SCAMP's rotors on at maximum, causing it to pivot around the tail's contact point and pitch toward the surface. Once the robot is aligned with the wall and the initial vibrations of impact have dissipated, the rotors spool down. This allows the feet to slide down along the wall and engage with the first available foothold.

This perching strategy is designed to meet two central challenges.

First, SCAMP perches using a mechanism that is highly weight-constrained and primarily designed for climbing. In order to climb using only two actuators, SCAMP takes advantage of directional attachment technology [15], [17]. The microspines adhere when pulled down against an asperity and release simply by removing the downward force, which helps create a smooth climbing gait. However, the impacts involved in perching often result in the spines experiencing forces that cause unintentional detachment. For this reason, previous perching work based on directional attachment had to use a soft carefully tuned suspension to prevent the robot from bouncing off

Authorized licensed use limited to: UNIVERSITA TRENTO. Downloaded on October 26,2022 at 09:44:36 UTC from IEEE Xplore. Restrictions apply.

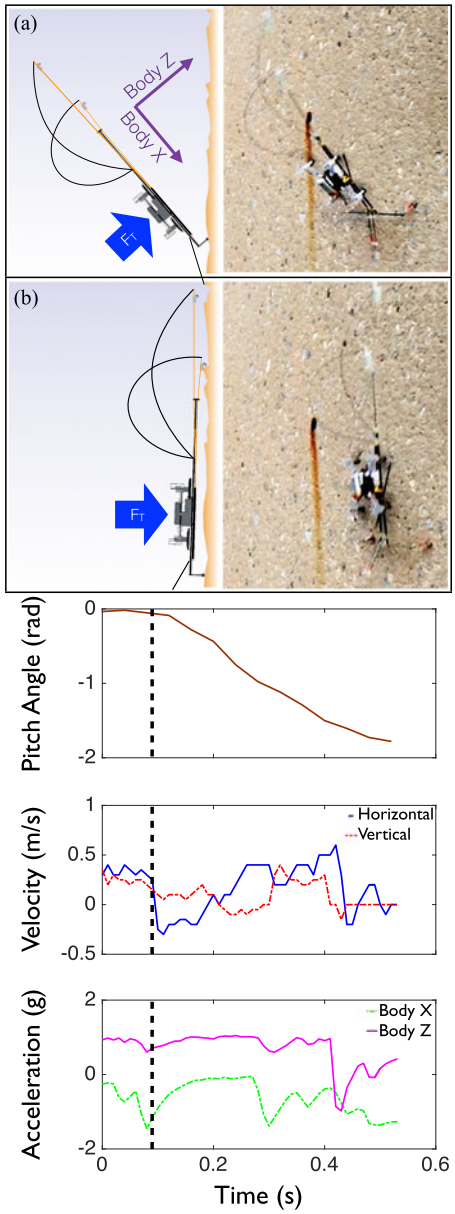

Fig. 3. (Top) Perching sequence: (a) SCAMP impacts a surface, pitches forward, and rotates. (b) Once aligned with the wall, it translates downward in search of an asperity. On the left is a cartoon depiction of the event; on the right are still shots from a video of an actual perch. (Bottom) Angle, velocity, and acceleration from a typical perch. Impact occurs around 0.1 s, as represented by the dashed vertical black line.

the wall [1]. To avoid the additional weight and complexity of such a suspension, SCAMP must use a perching strategy that is tolerant of the feet bouncing in and out of contact with the wall during the first milliseconds after impact.

To address this first challenge, SCAMP's climbing mechanism is mounted on top of the robot as it flies. This means that the aerodynamic force from the rotors is naturally oriented to press the robot into the wall. This aerodynamic force keeps the robot in contact with the wall as it comes to rest and begins to slide down along the target surface.

The second challenge SCAMP faces is to perch outdoors using only onboard sensing and computation. Ideally, SCAMP's

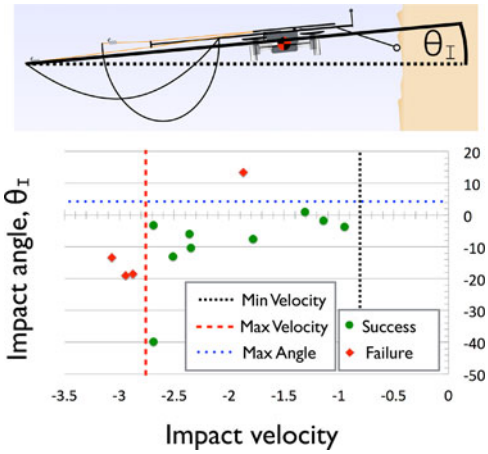

Fig. 4. (Top) Illustration of impact angle θ_I. (Bottom) Observed range of impact angles and velocities required for successful perching.

perching approach should be able to approach the wall at a variety of speeds, reliably execute the perching maneuver at the correct time, and then determine whether attachment has succeeded or failed.

To address this challenge, we use SCAMP's tail as a means of detecting the wall and also as a passive mechanical aid to achieve the appropriate perching maneuver. When SCAMP approaches a surface, the tail contacts first. Since the tail is stiff, this produces a large accelerometer signal, typically > 1.0 g, that triggers SCAMP's perching maneuver. The perching maneuver itself involves pitching the robot into the wall until the feet contact the surface and, at its simplest, can be accomplished by disabling the internal stabilization loop and turning the rotors to maximum thrust. As long as the point of impact is below the center of mass, the tail will exert a moment on the quadrotor, which acts to rotate it in the appropriate direction. Once the rotors are near the wall, ground effects act to pull SCAMP tightly against the surface.

This approach is most similar to that used in [9], which first attaches from the side and then pitches up to attach to a surface. Side attachment is not necessary in our case.

SCAMP can detect failure to attach by observing if vertical acceleration is less than 0.8 g a few hundred milliseconds after the initial impact with the wall.

A typical perch is illustrated in Fig. 3. The robot flies until the tail impacts the wall and allows it to detect the collision (a); then, the rotors apply maximum thrust, rotating the robot around the contact point to bring the feet into contact with the surface (b). This approach is robust within some angle and velocity constraints. At impact angles $\theta_I > 5^\circ$, the point of impact is above the center of mass (see Fig. 4), and torque is initially applied in the wrong direction, increasing the chance of failure. The impact velocity must also be large enough to create an acceleration above that experienced during normal flight conditions. Approximately, 1 g is a safe acceleration threshold, corresponding to $\approx$0.8 m/s. More advanced detection methods, such as ultrasonic or infrared distance sensing, could potentially reduce this limit to near zero. Initial velocities above $\approx$2.8 m/s produce large vibrations and a large initial rebound, which can lead to

Authorized licensed use limited to: UNIVERSITA TRENTO. Downloaded on October 26,2022 at 09:44:36 UTC from IEEE Xplore. Restrictions apply.

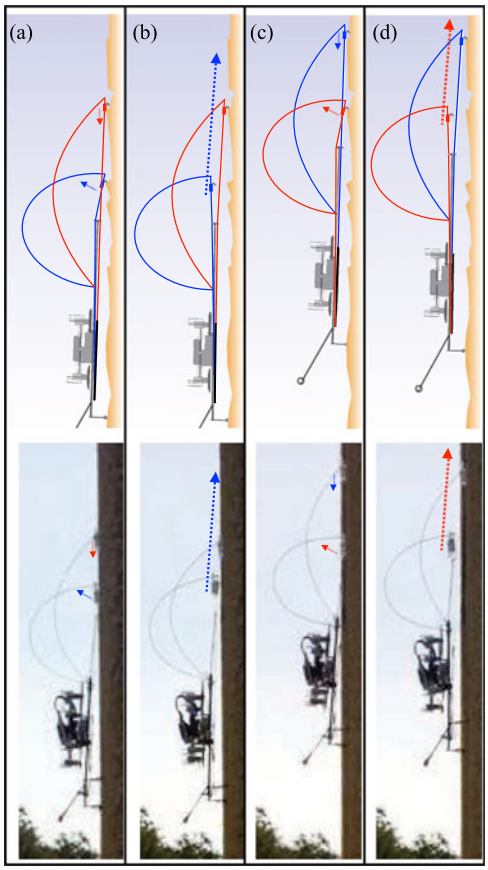

Fig. 5. Climbing sequence, in schematic view (top) and recorded images (bottom). (a) Top foot (drawn in red) is pressed into the wall, but has not yet engaged an asperity—SCAMP's weight is still supported by the bottom foot (drawn in blue). (b) Red foot engages an asperity, and the blue foot is released. (c) Extend/retract servo rotates, moving the blue foot upward past the red foot. The blue foot is then pushed back into the wall by the in/out guide. (d) Blue foot moves down and engages an asperity, allowing the red foot to disengage from the wall and move up.

SCAMP aligning incorrectly. Future perching algorithms could detect such large accelerations, abort the maneuver, and attempt a more gentle second approach. The current limits are summarized in Fig. 4.

C. Climbing Strategy

SCAMP's climbing strategy was chosen primarily with lightness and simplicity in mind, thus using the minimum number of feet and leveraging the asymmetric properties of angled spines to reduce gait complexity, as in [17]. The robot climbs by alternating the loads between its two feet, as illustrated in Fig. 5. This is similar to the climbing strategy used in [18] and [19], but the feet are close together and so do not exhibit similar dynamic swinging characteristics. A typical sequence is illustrated in Fig. 5 and begins with one foot (drawn in blue) engaged and at the bottom of its travel. The other foot (drawn in red) is at the top of its travel and is being pressed into the wall by the in/out guide. This means that the blue foot is being pulled slightly away from the wall by the in/out servo. In Fig. 5, this corresponds to diagram (a), with the blue foot engaged and the red foot contacting the wall but not yet locked on to an asperity. The extend/retract servo then begins to rotate, pulling the red foot down until it engages with a usable foothold. As the extend/retract servo continues to rotate, SCAMP's weight is transferred to the red foot and the blue foot releases from the wall, as pictured in diagram (b) of Fig. 5. The extend/retract servo rotates until the blue foot is at the top of its travel. Then, the in/out servo rotates to press the blue foot into the wall, simultaneously pulling the red foot away from the wall, as seen in diagram (c) of Fig. 5. The extend/retract servo then starts the next step by beginning to rotate in the opposite direction, transferring load to the blue foot and allowing the red foot to detach from the wall, as shown in diagram (d) of Fig. 5. A single step can be reliably executed in about 3 s, lifting the robot 9 cm up the wall and resulting in an average speed of 3 cm/s. Higher speeds tend to produce more vibrations and hence more frequent missed steps; in one set of trials on roofing shingle, a $3\times$ increase in climbing velocity corresponded to a $30 \pm 15\%$ (10) reduction in mean steps between failures.

On roofing shingle, the robot averages 18 ± 12 (20) steps between failures. On a stucco surface with more rounded asperities, this is reduced to 5 ± 4 (20), corresponding to an average height gain of $\approx$0.5 m between failures.

The basic climbing strategy can be modified by changing the motion of the two servo motors in order to produce different results. For instance, if the upper foot is engaged, load can be transferred to the lower foot, and then, the lower foot can be extended, moving the robot downward along the wall. Because SCAMP is capable of detecting and recovering gracefully from most climbing failures (see Section III-B), it is also possible in future work to adjust the climbing gait dynamically in the field. If SCAMP is having difficulty negotiating a specific surface, it could vary the angle of approach, the stroke length, or the amount of pressing force it uses when switching between feet, and observe whether failure incidence is reduced. For instance, on surfaces with large bumps or pits, climbing could be improved by minimizing the time with both feet near the surface to keep the unengaged spine from impacting overhanging asperities and causing vibrations; conversely, on surfaces with small sparse asperities, keeping both feet near the surface gives the top foot longer to find and engage with a useable foothold. For reasons outlined below, larger stroke length is generally desirable; however, on surfaces with low friction coefficients, a shorter stroke length may actually improve overall reliability.

As noted for various climbing robots (e.g., [10], [20], [21]), a tail reduces the pull-in force required at the feet to counteract the pitch-back moment produced by a center of mass that is some distance from the wall surface

$$F_A = W\left(\frac{d_{\mathrm{CM}}}{L_R}\right) \tag{1}$$

where F_A is the required force of adhesion, W is the weight of the robot, L_R is the length of the robot along the wall, and d_{CM} is the distance from the center of mass to the surface.

Authorized licensed use limited to: UNIVERSITA TRENTO. Downloaded on October 26,2022 at 09:44:36 UTC from IEEE Xplore. Restrictions apply.

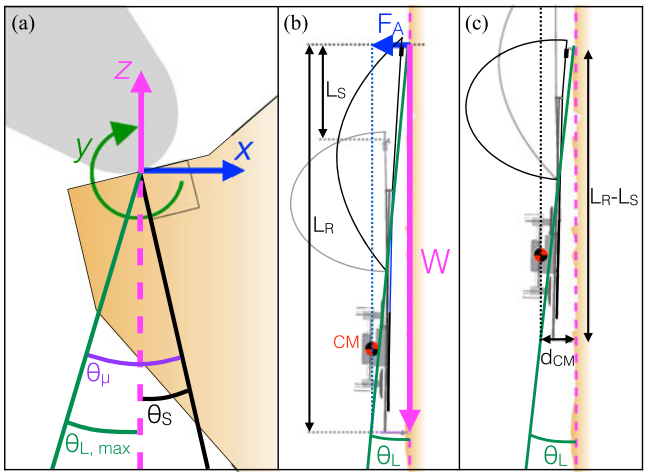

Fig. 6. (a) Single spine tip, with 10-μm tip radius, is engaged with an (exaggerated) asperity. Maximum loading angle, $\theta_{L,\max}$, is a function of the angle between the negative normal vector and vertical, θ_S, and $\theta_\mu = \tan^{-1}\mu$. (b) Loading angle, θ_L, is a function of the weight of the robot, W, and the force of adhesion at the spine, F_A. The size of the stroke length, L_S, relative to the length of the robot, L_R, determines the change in loading angle over a step. (c) End of a stroke. The loading angle is set by the distance from the engaged foot to the tail, $L_R - L_S$, and the distance from the center of mass to the wall, d_{CM}. The increase in θ_L can cause failure if the asperity is on the border of usability.

The required adhesive force can then be used to calculate the loading angle θ_L

$$\theta_L = \tan^{-1}\left(\frac{F_A}{W}\right). \tag{2}$$

For a foothold to be usable, θ_L must remain below an upper bound, $\theta_{L,\max}$

$$\theta_{L,\max} < \theta_S + \theta_\mu \tag{3}$$

where $\theta_\mu = \tan^{-1}\mu$, μ is the coefficient of friction between the spine and an asperity, and θ_S is defined as the angle from vertical down to the negative normal surface vector [see Fig. 6(a)]. All angles are signed using the right-hand rule with respect to the y-axis.

By minimizing θ_L, we can increase the number of usable asperities for a given surface profile [15]. To accomplish this, SCAMP climbs with its center of mass held close against the wall and uses both long legs and a long tail to minimize the required pull-in or adhesive force. SCAMP can also use aerodynamic forces to change the effective θ_L, as discussed further in Section III-A.

The adhesion considerations present us with a tradeoff in designing the stroke length for a step. Since the spines typically need some amount of travel before engaging with a surface asperity, a longer stroke means that proportionally less time and effort is wasted before finding asperities, and the majority of the stroke is used to propel the robot along the wall. Also, by requiring fewer steps to traverse an equivalent distance, a longer stroke length reduces the possibility of engaging a weak section of the surface that holds momentarily and then breaks. Thus, a longer stroke length increases the efficiency and reliability of climbing. However, a longer stroke length also means that there will be a relatively large change in the distance between the foot and the tail with each stroke. This change in distance increases the loading angle, as illustrated in Fig. 6, increasing the pitch-back moment and requiring a higher adhesive force. Because of these higher forces, a foothold that is initially usable might become untenable by the end of the stroke. Therefore, while increasing stroke length reduces the time spent searching for footholds and reduces the chance of failing on weak asperities, it also increases the chance that a foothold will fail mid-stroke due to changing loading angle; we must weigh these competing consequences in selecting an appropriate stroke length for SCAMP.

This problem is mitigated by the fact that the coefficient of friction is usually different when the foot is traveling along a surface trying to engage with an asperity (dynamic friction) than it is when the spine is already at rest on a usable foothold (static friction). When the foot is traveling along a wall, it will only stop when it encounters an area where the surface tangent, θ_S, is at a large enough angle to provide a foothold based on dynamic friction. Once the foot has stopped against this asperity, however, it enters the static friction regime. Since the static friction coefficient, μ_s, is generally larger than the dynamic friction coefficient, μ_d, this usually means that the asperity will be able to tolerate an increase in θ_L. If the static and dynamic friction coefficients are known, the allowable increase in θ_L can be calculated as

$$\Delta\theta_L = \tan^{-1}\mu_s - \tan^{-1}\mu_d. \tag{4}$$

This relationship allows us to approximate the maximum allowable stroke length, L_S, in terms of L_R, μ_s, μ_d, and $r_{dL} = \frac{d_{CM}}{L_R}$, as derived in detail in Appendix A as

$$L_{S,\max} \approx \frac{1}{1 + r_{dL}\frac{1+\mu_s\mu_d}{\mu_s-\mu_d}} L_R, \quad r_{dL} \ll 1. \tag{5}$$

We can now see that maximum stroke length increases as the difference between μ_s and μ_d increases, and for robot designs with a smaller r_{dL}.

SCAMP's stroke length was initially designed simply for maximum travel given motor torque constraints. The analysis conducted here predicts that it will function well on surfaces with a spine-to-surface static friction coefficient greater than 0.2 and a difference between static and dynamic friction of at least 20%, which in practice includes most rough exterior surfaces.

D. Takeoff Strategy

When it is time to return to free flight, SCAMP must rotate away from the wall. Since all four rotors are located above the tail's contact point with the wall, they cannot exert the necessary righting moment by applying positive thrust. This means that even if SCAMP could disengage both of its feet, it would be unable to rotate and would fall down along the wall until it impacted a horizontal surface. One solution is to modify the motor drive circuitry to allow for driving the rotors in reverse for short periods of time. In the current implementation, however,

Authorized licensed use limited to: UNIVERSITA TRENTO. Downloaded on October 26,2022 at 09:44:36 UTC from IEEE Xplore. Restrictions apply.

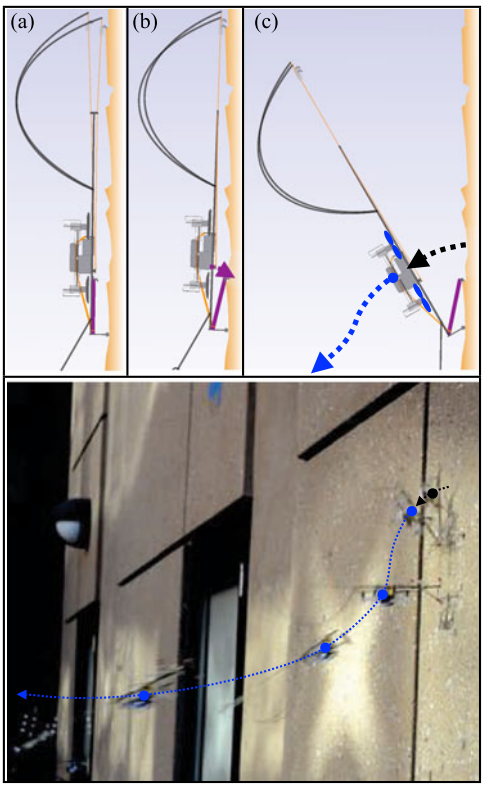

Fig. 7. Schematic of SCAMP's takeoff mechanism. (a) During normal operation, the takeoff arm is held away from the wall. (b) When both servos are rotated to a special position not seen during normal climbing, the takeoff arm deploys and contacts the surface. (c) Load is transferred to the takeoff spine, causing the robot to pitch back away from the wall.

we use a mechanical solution to generate the necessary righting moment, illustrated in Fig. 7.

The mechanical solution uses a "takeoff arm" mounted via a pin joint to the tail. At the end of this takeoff arm is a single spine. During climbing, the takeoff arm is kept close to the carbon fiber frame, away from contact with the wall. When takeoff is desired, both servos move to a combined position not encountered during normal climbing operation to release the takeoff arm and allow its attached spine to contact the wall, as described further in Appendix B. The up/down servo then moves to release tension from whichever foot is currently engaged, allowing the robot to move downward and causing the takeoff spine to drag along the surface. When the spine on the takeoff arm engages an asperity, load is transferred from the engaged foot to it, causing the robot to pitch backward from the wall. When SCAMP detects a change in angle $>40^\circ$, it turns the rotors on and flies up and away from the wall, disengaging the takeoff spine and returning to normal flight.

E. Flight Performance

The addition of the perching and climbing mechanism reduces the flying performance of the Crazyflie. Performance of the bare Crazyflie 2.0 platform has been described in detail in [22]. The increased mass of SCAMP's mechanism reduces flight time by 50% and thrust-to-weight ratio by 40%. Because the tail and feet are extended significantly from the center of mass, the mechanism has an even larger impact on moment of inertia, especially in the pitch axis. In [22], inertia in this axis was calculated to be 2.4×10^{-5} kg$(\cdot)$m^2. We calculate that SCAMP's mechanism increases the total inertia to 1.1×10^{-4} kg$(\cdot)$m^2, or 4.6$\times$ the original value. We verified the effect on rotational performance by observing the time required to pitch 35° at maximum control input with and without the mechanism and assuming a constant angular acceleration throughout each maneuver. Without the mechanism, average angular acceleration was observed to be 280 rad/s^2. With the mechanism, average angular acceleration was 4.4$\times$ smaller, or 63 rad/s^2.

III. Rotor-Assisted Climbing

A hybrid aerial–scansorial robot has unique access to aerodynamic forces while climbing. In this section, we examine two ways, in which the rotors used primarily for flying can improve climbing performance. First, we examine how rotor thrust can change the effective angle with which a microspine interacts with a surface and how this can increase the apparent density of asperities. Second, we discuss how the ability to fly safeguards the robot against occasional climbing failures and report the empirical results of recovery tests in operation.

A. Using Rotor Thrust to Increase Asperity Density

As discussed in Section II-C, in order for a given foothold to be usable, the loading angle must be below a threshold that depends on the surface angle, θ_S, and the coefficient of friction, μ [see (3)]. For a conventional climbing robot, where θ_L is purely a function of the robot's geometry, knowledge of μ and the swept surface profile is sufficient to determine the number of usable asperities in a given region. We solve (3) for θ_S to find the minimum graspable surface angle

$$\theta_S > \theta_L - \theta_\mu. \tag{6}$$

Note that we cannot simply use the bare surface profile because the spine tip radius ($\approx 10\,\mu$m) creates a traced surface [23] that effectively smooths the surface profile [15]. Fig. 8(a) shows a 150 μm-long section of concrete and the traced surface for a spine from [15]. For a loading angle of $\approx 7^\circ$ and μ of ≈ 0.2, there are just three usable regions, which are representative of the average asperity density for this surface.

SCAMP, however, can apply thrust to change the loading angle

$$\theta_L = \operatorname{atan}\left(\frac{F_A - T}{W}\right) \tag{7}$$

where T is the thrust of the rotors into the wall. With a small amount of thrust, it is possible to greatly increase the number of usable asperities [see Fig. 8(b)]. Here, ≈ 0.25 body weights of thrust are added, resulting in the number of useful asperities increasing from 3 to 8. The solution is reminiscent of flightless birds that use wings to run up vertical surfaces [24] and robotic platforms that use thrust to increase frictional forces for climbing [25].

Authorized licensed use limited to: UNIVERSITA TRENTO. Downloaded on October 26,2022 at 09:44:36 UTC from IEEE Xplore. Restrictions apply.

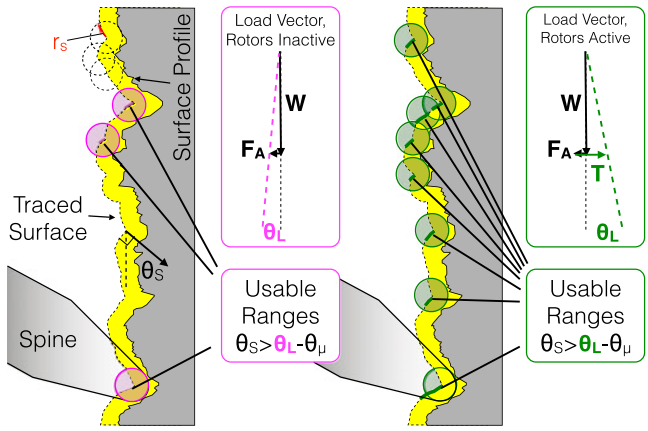

Fig. 8. (a) In grasping a surface with spines, only areas of the surface with a sufficiently shallow slope are usable for a loading angle, θ_L. (b) When thrust is added, θ_L rotates into the wall, resulting in a smaller lower bound on the surface angle, θ_S, from (6); this increases both the number and length of available asperities. Concrete profile is taken from [15].

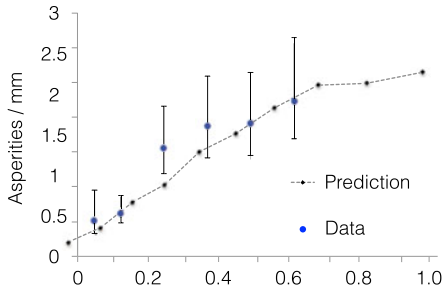

Fig. 9. Adding a small amount of thrust during climbing significantly increases the number of usable asperities. Predicted performance is based on concrete data from [15] and is approximately matched by dragging a spine along randomly selected paths on a concrete cinderblock (160 total trials). Thrust $\approx 1/4$ body weight provides $> 3\times$ usable asperity density.

More generally, taking the concrete profiles recorded in [15] and a 10-μm spine tip radius, we can compute how the density of asperities will change as the loading angle is changed. This calculation provides the predicted performance graphed in Fig. 9. Additional surfaces measured in [15] show similar trends, but of the surfaces measured in that paper, concrete cinderblock showed the most dramatic relationship between loading angle and asperity density, which makes it ideal for demonstrating the possible benefits.

To verify this model, we dragged a single microspine along a concrete cinderblock with varying ratios of shear to normal loading forces. We measured the average distance to find an asperity and, then, took the inverse of that number to estimate the number of asperities per millimeter. The results are plotted against our prediction in Fig. 9. If the distance between asperities is modeled as a Poisson random variable (as in [15]), then the distribution of the traveling distance of a single spine on a surface before engaging an asperity follows an exponential distribution

$$f(\lambda; x) = \lambda e^{-\lambda x}, \qquad x \geq 0 \tag{8}$$

where x is the distance traveled, and λ is the number of asperities per unit length. As λ increases, the exponential function decays more rapidly, meaning long travel distances become less likely.

The error bars in Fig. 9 represent the 95% confidence intervals for our estimate of the mean given an exponential distribution. Note that the cinderblock used in Fig. 9 does not have the exact same surface profile, as that recorded in [15], so some variation is expected.

Early in the development of SCAMP, experiments were conducted with a 4-g shroud around the rotors so that suction effects created forces approximately one-fourth of SCAMP's weight, while requiring only 10% of the maximum rotor power. As seen in Fig. 9, this is sufficient to triple the usable asperity density. In the final version, the shroud has been omitted, as 4 g is a significant weight penalty for flying and the thrust obtained at 10% rotor power without the shroud is enough to improve climbing performance.

For example, SCAMP misses an average of one out of every 18 ± 12 (20) steps on composite roofing shingle, an asperity-rich surface in comparison to concrete. However, with the rotors at 10% of their maximum power (without a shroud), ten trials of $\sim$30 steps each were taken with no missed steps. For a more challenging surface, the increase in asperity density, and subsequent reduction in time and energy spent searching for a good grip, might outweigh the cost of engaging the rotors; demonstrating this experimentally is a task for future work. At present, the surfaces studied did not require the use of the rotors for effective traversal.

B. *Using Rotors as a Fail-Safe for Climbing*

Many climbing animals, regardless of whether they are capable of flight, use aerodynamic forces to mitigate the effects of a climbing failure [26]. Flight, including gliding and parachuting, is among the most robust of failure responses, and the addition of flight capability to a climbing robot has many implications. The robot is now able to attempt surfaces of questionable tractability, characterize those surfaces, and do so without fear of catastrophic failure.

In addition to allowing the robot to fly away, SCAMP's rotors can be used to help reengage with a surface after a missed step, as illustrated in Fig. 10. Using the onboard accelerometer, SCAMP can detect a free-fall condition; during our experiments, the robot's rotors started turning within 10 ms of detachment. Since most failure events do not impart a large velocity away from the wall, a small amount of thrust will quickly return the robot to contact with the surface, allowing it to engage with a new asperity and arrest its descent. Average fall distance on stucco is 14 ± 12 cm (10).

The addition of this recovery capability means that SCAMP has much greater flexibility in the kind of surfaces it can attempt to traverse. If it encounters a difficult surface, it is unlikely to fail catastrophically and can respond by tuning its gait, as discussed in Section II-C, or by increasing rotor thrust, as described in Section III-A.

IV. Power and Energy Considerations

A commonly cited motivation for perching is to extend mission life. While perched, climbing can be used to change position on the surface without having to take off and reattach.

Authorized licensed use limited to: UNIVERSITA TRENTO. Downloaded on October 26,2022 at 09:44:36 UTC from IEEE Xplore. Restrictions apply.

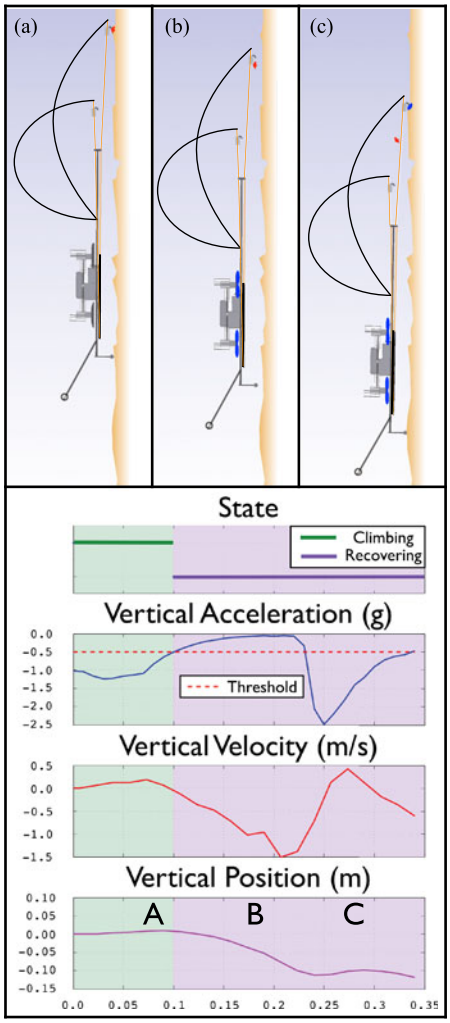

Fig. 10. Recovery strategy: (a) SCAMP begins to fall when its grip on an asperity fails. (b) On detection of reduced vertical acceleration, SCAMP's rotors ramp up to push the robot toward wall. (c) Robot contacts surface and engages a new asperity. (Bottom) Data for a typical fall collected using onboard sensors (acceleration, internal state) and video (vertical position, velocity). When acceleration < 0.5 g, SCAMP begins recovery by increasing rotor thrust, which returns SCAMP to wall for reengagement.

Climbing requires less power than flying, but whether it requires less energy per unit distance has not previously been measured.

To evaluate the possible mission life extension from our current perching setup, we measured real current draw in a variety of scenarios. SCAMP is not optimized for energy or power efficiency, so these numbers serve merely as a quantitative baseline for future work. Power draw is minimal for the case in which SCAMP is at rest on the wall without using its radio and increases as additional systems come online, as illustrated in Fig. 11.

The computation and sensing units on the Crazyflie platform are not optimized to reduce power consumption, as the base load is in any case small against the costs of active hovering. Substantial losses also occur in the gear trains of the servos, which could be replaced with more efficient drives in future iterations. Also, since motor performance tends to scale favorably with

System Configuration	Power Draw	Energy to Move Up 1 m	Time of Operation on Single Charge
Perched with Processor and Radio on	.5 W	N/A	105 min.
Climbing (3 cm/s)	1.1 W	37 J	50 min.
Climbing with rotors on at 10%	2.7 W	90 J	20 min.
Flying at maximum thrust (1 m/s)	15 W	15 J	3.5 min.
Take off, fly up, re-perch	15 W	45 J	3.5 min.

Fig. 11. Power and energy considerations: power draw was measured for each system configuration, and the energy to translate 1 m upward is compared for the three locomotion modes. Time of operation is calculated using measured power draw and rated battery life. Energy use for taking off and reperching is calculated using the conservative assumption that an extra second of flight time is required for both takeoff and perching maneuvers.

increasing size [27], a larger platform might climb more efficiently. Fundamentally, climbing involves less work than flying, because the robot only needs to move itself when climbing, as opposed to the need to also accelerate air in order to generate thrust for flying. Hence, it is possible that with future modifications, climbing could become as efficient for covering short distances as flying.

V. Discussion

Multimodal operation generally implies compromises in order to incorporate two independent forms of locomotion. In the current case, a climbing mechanism represents additional weight during flying and so must be optimized with respect to weight as well as reliable operation. This is also true for climbing, where the bulk of the flying machine is unused in normal operation. However, compromises are also accompanied by certain synergies. As SCAMP demonstrates, the use of a flying platform can improve the reliability of climbing with microspines in a few important ways: the rotors can be turned ON to increase normal forces and the corresponding density of usable asperities on a wall; the rotors can also resist vibrations that might otherwise cause failure to attach, and if a fall occurs, they can be used to quickly reattach and resume climbing.

At the same time, an ability to perch allows the extension of mission life by reducing power draw, thus increasing the capability of the flying robot to achieve certain missions.

VI. Conclusion and Future Work

SCAMP demonstrates mechanisms and strategies that allow for perching, climbing, takeoff, and failure recovery on rough exterior surfaces with only onboard sensing. The robot exploits the fact that the sensitive accelerometers used in flying are also useful for detecting relevant events for perching, climbing, takeoff, and recovery. Because of its multimodal capabilities, SCAMP introduces new strategies for climbing that are unavailable to a flightless climbing robot. Carrying a climbing

Authorized licensed use limited to: UNIVERSITA TRENTO. Downloaded on October 26,2022 at 09:44:36 UTC from IEEE Xplore. Restrictions apply.

mechanism reduces flying maneuverability in general, but can improve the operation of certain maneuvers like perching. Likewise, carrying a flying platform requires more mechanical work from a climbing robot, but having the ability to generate aerodynamic forces can improve the reliability of climbing. The ability to perch can extend the mission life of SCAMP from minutes to hours and could have an even more dramatic effect if measures were taken to reduce computational power draw and losses in the servo gear train.

In future work, we will explore the possibility of scaling up the platform. The current mechanism could be attached directly to a slightly larger quadrotor as long as stroke length was reduced to stay within the torque limits of the current servo. Scaling up beyond a factor of 2 or 3 would require a new servo and possibly more load-sharing between spines on the feet.

Other future work will use SCAMP's sensor inputs to actively tune climbing and perching strategies in the field as it encounters surfaces with more or fewer asperities. Mechanical improvements will also expand the range of surfaces that SCAMP can climb. In particular, the current mechanism cannot adapt to curvatures with a radius of <10 cm, nor can it move horizontally. A more adaptable gait with additional degrees of freedom would be desirable to allow these kinds of motions. This could be achieved through additional actuators or through clutches and transmission redesign.

Appendix A
Derivation of Maximum Stroke Length

In order for confidence to be placed in a foothold over the course of a stroke, the change in loading angle, θ_L, must be less than $\Delta\theta_L$

$$\Delta\theta_L > \tan^{-1}\left(\frac{d_{\text{CM}}}{L_R - L_S}\right) - \tan^{-1}\left(\frac{d_{\text{CM}}}{L_R}\right) \tag{9}$$

where L_R is the length of the robot along the wall, L_S is the stroke length, and d_{CM} is the distance from the center of mass to the surface [see Fig. 6(a)]. To solve for L_S, we first take the tangent of both sides

$$\tan\Delta\theta_L > \tan(\theta_{L2} - \theta_{L1}), \quad \text{where} \tag{10}$$

$$\theta_{L1} = \tan^{-1}\left(\frac{d_{\text{CM}}}{L_R}\right) \quad \text{and} \tag{11}$$

$$\theta_{L2} = \tan^{-1}\left(\frac{d_{\text{CM}}}{L_R - L_S}\right). \tag{12}$$

The tangent can then be expanded to yield the expression

$$\tan\Delta\theta_L > \frac{\sin\theta_{L2}\cos\theta_{L1} - \cos\theta_{L2}\sin\theta_{L1}}{\cos\theta_{L2}\cos\theta_{L1} + \sin\theta_{L2}\sin\theta_{L1}}. \tag{13}$$

Using the geometry of the original problem, we can make the following replacements for $\sin$ and $\cos$:

$$\sin\theta_{L1} = \frac{d_{\text{CM}}}{\sqrt{L_R^2 + d_{\text{CM}}^2}} \tag{14}$$

$$\cos\theta_{L1} = \frac{L_R}{\sqrt{L_R^2 + d_{\text{CM}}^2}} \tag{15}$$

$$\sin\theta_{L2} = \frac{d_{\text{CM}}}{\sqrt{(L_R - L_S)^2 + d_{\text{CM}}^2}} \tag{16}$$

$$\cos\theta_{L2} = \frac{d_{\text{CM}}}{\sqrt{(L_R - L_S)^2 + d_{\text{CM}}^2}}. \tag{17}$$

Substituting these expressions back into (13) and simplifying gives us the following expression:

$$\tan\Delta\theta_L > \frac{L_S d_{\text{CM}}}{L_R^2 + d_{\text{CM}}^2 - L_S L_R}. \tag{18}$$

Before solving for L_S, we can remove trigonometric equations from the left side of the equation by first expanding $\Delta\theta_L$ as

$$\tan\Delta\theta_L = \tan(\theta_{\mu_s} - \theta_{\mu_d}) \tag{19}$$

where θ_{μ_s} is $\tan^{-1}\mu_s$ and θ_{μ_d} is $\tan^{-1}\mu_d$. We can expand this

$$\tan\Delta\theta_L > \frac{\sin\theta_{\mu_s}\cos\theta_{\mu_d} - \cos\theta_{\mu_s}\sin\theta_{\mu_d}}{\cos\theta_{\mu_s}\cos\theta_{\mu_d} + \sin\theta_{\mu_s}\sin\theta_{\mu_d}} \tag{20}$$

and then using

$$\sin\theta_{\mu_d} = \frac{\mu_d}{\sqrt{1+\mu_d^2}} \tag{21}$$

$$\cos\theta_{\mu_d} = \frac{1}{\sqrt{1+\mu_d^2}} \tag{22}$$

$$\sin\theta_{\mu_s} = \frac{\mu_s}{\sqrt{1+\mu_s^2}} \tag{23}$$

$$\cos\theta_{\mu_s} = \frac{1}{\sqrt{1+\mu_s^2}} \tag{24}$$

we can simplify and solve for a new expression for the left-hand side of the equation

$$\tan\Delta\theta_L = \frac{\mu_s - \mu_d}{1 + \mu_s\mu_d}. \tag{25}$$

Placing this back in the original equation, we now have

$$\frac{\mu_s - \mu_d}{1 + \mu_s\mu_d} > \frac{L_S d_{\text{CM}}}{L_R^2 + d_{\text{CM}}^2 - L_S L_R}. \tag{26}$$

If we now solve for L_S, we get a formula for the maximum stroke length based on the static and dynamic friction coefficients and the robot geometry

$$L_S < \frac{L_R^2 + d_{\text{CM}}^2}{L_R + \frac{d_{\text{CM}}(1+\mu_s\mu_d)}{\mu_s - \mu_d}}. \tag{27}$$

If we define r_{dL} as the ratio of d_{CM} to L_R, we can rearrange the limit on L_S as a quantity determined by r_{dL}, μ_s, and μ_d and

Authorized licensed use limited to: UNIVERSITA TRENTO. Downloaded on October 26,2022 at 09:44:36 UTC from IEEE Xplore. Restrictions apply.

scaled by the robot length L_R as

$$L_S < \frac{1 + r_{dL}^2}{1 + r_{dL}\frac{1+\mu_s\mu_d}{\mu_s - \mu_d}} L_R. \tag{28}$$

Since r_{dL} is designed to be $\ll 1$ in order to minimize θ_L and maximize the number of useable asperities, we can approximate the limit on L_S as

$$L_{S,\max} \approx \frac{1}{1 + r_{dL}\frac{1+\mu_s\mu_d}{\mu_s - \mu_d}} L_R, \quad r_{dL} \ll 1. \tag{29}$$

APPENDIX B
DETAILS OF TAKEOFF SPINE DEPLOYMENT

The takeoff arm is held away from the wall at any given time by one of two independent mechanical means. The first is a tendon attached to the takeoff arm near the pin joint and routed through the body of the robot to connect to an arm attached to the in/out servo. When the in/out servo is at the extreme ends of its motion, this "takeoff tendon" is taut, keeping the takeoff arm pressed against the body of the robot. When the in/out servo is in the middle of its travel, the tendon is slack.

The second method of restraining the takeoff arm uses a small carbon-fiber bar attached to the end of the takeoff arm. When the extend/retract servo arm is at the ends of its travel, it overlaps with this "locking bar," preventing the takeoff arm from swinging out toward the surface. When extend/retract servo is in the middle of its range, the bar is free to move.

Thus, the takeoff arm can only deploy when the takeoff tendon is slack and the extend/retract arm is out of the way of the locking bar. During normal climbing operation, the extend/retract arm is moved to a blocking position before the in/out servo removes tension on the takeoff tendon. The in/out servo then retensions the takeoff tendon before the extend/retract servo is allowed to move. When takeoff is desired, moving both servos simultaneously to the middle of their servo ranges allows the takeoff arm to rotate away from the body of the robot and into contact with the surface.

REFERENCES

[1] A. Lussier-Desbiens, A. T. Asbeck, and M. R. Cutkosky, "Landing, perching and taking off from vertical surfaces," *Int. J. Robot. Res.*, vol. 30, no. 3, pp. 355–370, 2011.

[2] E. W. Hawkes *et al.*, "Dynamic surface grasping with directional adhesion," in *Proc. IEEE Int. Conf. Intell. Robot Syst.*, 2013, pp. 5487–5493.

[3] M. L. Anderson, B. M. H. C. J. Perry, D. S. Olsen, J. R. Parcus, K. M. Pederson, and D. D. Jensen, "The sticky-pad plane and other innovative concepts for perching UAVs," in *Proc. 47th AIAA Aerosp. Sci. Meeting*, 2009, pp. 40–51.

[4] D. Mellinger, M. Shomin, and V. Kumar, "Control of quadrotors for robust perching and landing," in *Proc. Int. Powered Lift Conf*, 2010, pp. 119–126.

[5] M. Kovac, J. M. Germann, C. Hurzeler, R. Siegwart, and D. Floreano, "A perching mechanism for micro aerial vehicles," *J. Micro-Nano Mechatronics*, vol. 5, pp. 77–91, 2009.

[6] L. Daler, A. Klaptocz, A. Briod, M. Sitti, and D. Floreano, "A perching mechanism for flying robots using a fibre-based adhesive," in *Proc. IEEE Int. Conf. Robot. Autom.*, 2013, pp. 4433–4438.

[7] C. E. Doyle *et al.*, "An avian-inspired passive mechanism for quadrotor perching," *IEEE/ASME Trans. Mechatronics*, vol. 18, no. 2, pp. 506–517, Apr. 2013.

[8] A. Kalantari, K. Mahajan, D. Ruffatto, III, and M. Spenko, "Autonomous perching and take-off on vertical walls for a quadrotor micro air vehicle," in *Proc. IEEE Int. Conf. Robot. Autom.*, 2015, pp. 4669–4674.

[9] H. Tsukagoshi, M. Watanabe, T. Hamada, D. Ashlih, and R. Iizuka, "Aerial manipulator with perching and door-opening capability," in *Proc. IEEE Int. Conf. Robot. Autom.*, 2015, pp. 4663–4668.

[10] M. Estrada *et al.*, "Perching and vertical climbing: Design of a multimodal robot," in *Proc. IEEE Int. Conf. Robot. Autom.*, 2014, pp. 4215–4221.

[11] W. Myeong, K. Jung, S. Jung, Y. Jung, and H. Myung, "Development of a drone-type wall-sticking and climbing robot," in *Proc. 12th Int. Conf. Ubiquitous Robots Ambient Intell.*, 2015, pp. 386–389.

[12] P. Beardsley *et al.*, "Disney vertigo," [Online]. Available: https://www.disneyresearch.com/publication/vertigo/, Accessed on: Feb. 4, 2016.

[13] J. D. Dickson and J. E. Clark, "Design of a multimodal climbing and gliding robotic platform," *IEEE/ASME Trans. Mechatronics*, vol. 18, no. 2, pp. 494–505, Apr. 2013.

[14] "Crazyflie nano quadcopter," [Online]. Available: https://www.bitcraze.io/crazyflie/, Accessed on: Aug. 30, 2015.

[15] A. T. Asbeck, S. Kim, M. R. Cutkosky, W. R. Provancher, and M. Lanzetta, "Scaling hard vertical surfaces with compliant microspine arrays," *Int. J. Robot. Res.*, vol. 25, no. 12, pp. 1165–1179, 2006.

[16] B. Brown and G. Zeglin, "The bow leg hopping robot," in *Proc. IEEE Int. Conf. Robot. Autom.*, May 1998, vol. 1, pp. 781–786.

[17] E. W. Hawkes, D. L. Christensen, and M. R. Cutkosky, "Vertical dry adhesive climbing with a 100x bodyweight payload," in *Proc. IEEE Int. Conf. Robot. Autom.*, 2015, pp. 3762–3769.

[18] J. Clark *et al.*, "Design of a bio-inspired dynamical vertical climbing robot," in, *Robotics: Science and Systems*. Cambridge, MA, USA: MIT Press, 2007.

[19] J. Dickson and J. Clark, "The effect of sprawl angle and wall inclination on a bipedal, dynamic climbing platform," in *Adaptive Mobile Robotics: Proceedings of the 15th International Conference on Climbing and Walking Robots and the Support Technologies for Mobile Machines*. Singapore: World Scientific, 2012, p. 459.

[20] A. T. Asbeck and M. R. Cutkosky, "Designing compliant spine mechanisms for climbing," *ASME J. Mech. Robot.*, vol. 4, no. 3, 2012, Art. no. 031007.

[21] C. Menon, M. Murphy, and M. Sitti, "Gecko inspired surface climbing robots," in *Proc. IEEE Int. Conf. Robot. Biomimetics*, 2004, pp. 431–436.

[22] B. Landry, "Planning and control for quadrotor flight through cluttered environments," master's thesis, Massachusetts Inst. Technology, Cambridge, MA, USA, 2015.

[23] A. M. Okamura and M. R. Cutkosky, "Feature detection for haptic exploration with robotic fingers," *Int. J. Robot. Res.*, vol. 20, no. 12, pp. 925–938, 2001.

[24] K. P. Dial, "Wing-assisted incline running and the evolution of flight," *Science*, vol. 299, no. 5605, pp. 402–404, 2003.

[25] J.-U. Shin, D. Kim, J.-H. Kim, and H. Myung, "Micro aerial vehicle type wall-climbing robot mechanism," in *Proc. IEEE RO-MAN*, 2013, pp. 722–725.

[26] S. P. Yanoviak, Y. Munk, M. Kaspari, and R. Dudley, "Aerial manoeuvrability in wingless gliding ants (cephalotes atratus)," *Proc. Roy. Soc. London B, Biol. Sci.*, vol. 277, pp. 2199–2204, 2010.

[27] R. J. Wood *et al.*, "Progress on pico air vehicles," *Int. J. Robot. Res.*, vol. 31, no. 11, pp. 1292–1302, 2012.

Morgan T. Pope received the Bachelor's degree in engineering sciences from Harvard University, Cambridge, MA, USA, and the Master's and Doctorate degrees in mechanical engineering from Stanford University, Stanford, CA, USA.

His research focuses on novel robotic locomotion strategies.

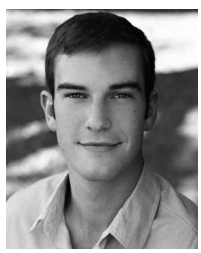

Christopher W. Kimes is working toward the B.S. in mechanical engineering at Stanford University, Stanford, CA, USA. He plans to pursue a Master's degree in mechanical engineering with a focus on mechatronics.

His research interests include mechatronics, controls, and mechanism design.

Authorized licensed use limited to: UNIVERSITA TRENTO. Downloaded on October 26,2022 at 09:44:36 UTC from IEEE Xplore. Restrictions apply.

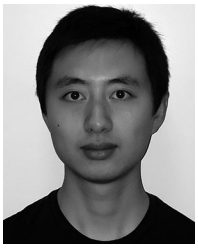

Hao Jiang received the B.S. degree in mechanical engineering from Beijing University of Aeronautics and Astronautics, Beijing, China, in 2012 and the M.S. degree in mechanical engineering from Stanford University, Stanford, CA, USA, in 2014. He is currently working toward the Ph.D. degree in mechanical engineering in the Biomimetics and Dexterous Manipulation Laboratory, Stanford University.

His research interests include applying bio-inspired adhesive technology such as gecko adhesives and microspines to robotic gripper designs, as well as UAV perching and sensing strategies with machine learning.

Mr. Jiang received one ICRA Best Paper Award and two IROS Best Paper Awards as a co-author.

Elliot W. Hawkes (S'11) received the B.S. degree with highest honors in mechanical engineering from Harvard University, Cambridge, MA, USA, in 2009, and the M.S. degree in 2012, the Ph.D. degree, under Prof. Mark Cutkosky, in mechanical engineering in 2015, both from Stanford University, Stanford, CA, USA.

He is an Assistant Professor of mechanical engineering with University of California, Santa Barbara, CA, USA. His research interests include compliant robot body design, mechanism design, nontraditional materials, artificial muscles, directional adhesion, and growing robots.

He was a Rhodes Scholar Finalist, a National Defense Science and Engineering Graduate Fellow, and a National Science Foundation Graduate Research Fellow.

Matt A. Estrada received the B.S. degree in mechanical engineering from Massachusetts Institute of Technology, Cambridge, MA, USA, in 2012 and the M.S. degree in mechanical engineering from Stanford University, Stanford, CA, USA, in 2015.

Capella F. Kerst received the Bachelor's degree from University of California, Berkeley, CA, USA, and the Master's degree from University of California, Los Angeles, CA, USA. She is currently working toward the Ph.D. degree in mechanical engineering under the supervision of Professor Mark Cutkosky at Stanford University.

William R. T. Roderick received the B.S. degree in mechanical engineering from Stanford University, Standford, CA, USA, in 2016. He is currently working toward the Ph.D. degree in mechanical engineering at Stanford University.

He received the National Science Foundation Graduate Research Fellowship Program Award in 2016.

Amy K. Han received the Bachelor's degree in mechanical engineering from Georgia Institute of Technology College of Engineering, Atlanta, GA, USA, in 2012 and the Master's degree in mechanical engineering from Stanford University, Stanford, CA, USA, in 2015. She is working toward the Ph.D. degree in mechanical engineering at Stanford University.

Her research interests include bio-inspired robotics, electroactive polymers, and haptics.

David L. Christensen is working toward the Ph.D. degree in mechanical engineering.

Before coming to Stanford for the graduate degree, he served as Director of Research and Development, Valimet, Inc., Stockton, CA, USA, a manufacturer of micron-sized spherical metal powders used in applications including aerospace (solid rockets and turbine blades), metallic 3-D printing, automobile airbags, solar panels, and metallic pigments. His research interest focused on mechatronics, MEMS, smart materials and biomechanics in his time at Stanford. He worked on synthetic gecko adhesives, robotic sensors, and microrobotics with Prof. Mark Cutkosky as well as the design of resonant MEMS sensors with Prof. Tom Kenny. David is also an Accel Innovation Scholar, a Stanford program built to enable late stage graduate students with the tools needed to undertake entrepreneurial endeavors such as bringing their research out of lab and into the world.

Mark R. Cutkosky (F'12) received the Ph.D. degree in mechanical engineering from Carnegie Mellon University, Pittsburgh, PA, USA, in 1985.

He is the Fletcher Jones Professor in the Department of Mechanical Engineering, Stanford University, Stanford, CA, USA. His research interests include bio-inspired robots, haptics, and rapid prototyping processes. Dr. Cutkosky is a Fellow of the ASME.

Dr. Cutkosky is a Fellow of the ASME.

Authorized licensed use limited to: UNIVERSITA TRENTO. Downloaded on October 26,2022 at 09:44:36 UTC from IEEE Xplore. Restrictions apply.